Published by The College of Vocational and Technology Education (COVTED), TASUED, vol. 20, no 1, pp. 37-45.

COVTED, TASUED
The Vocational and Applied Science Journal (VAS)

Variability Study of the Effect of Geomagnetic Storm of May, 10th - 11th, 2024 on the H-Component of the Geomagnetic Field using Wavelet Power Spectrum

[1]**Bamidele, K. J.,** [2]**Falayi, F. C.,** [3]**Kotoye, A. A.** [1]**Daini, P. A., and** [1]**Martins, S. O.**
[1]Department of Physics, Tai Solarin Federal University of Education, Ijagun, Ogun State, Nigeria
[2]Department of Computer Science, Federal University of Agriculture, Abeokuta, Nigeria
[3]Department of Science Laboratory Technology, Abraham Adesanya Polytechnic, Ijebu Igbo, Ogun State, Nigeria
Corresponding email: *adekayo23@gmail.com*

Abstract
The study investigated the variability of geomagnetic storms from May 10th – 11th 2024 in Sulari (Iceland), Sodankylä (Finland), Nurmijärvi (Finland), Lerwick (United Kingdom) and Eskdalemuir (United Kingdom) using Wavelet Power Spectrum (WPS). The geomagnetic storm is a disturbance that can disrupt satellite communications, navigation, power grid as well as human socio-economic activities. The geomagnetic disturbance of May 10th – 11th 2024 was caused by a Coronal Mass Ejection (CME). The impact of CME was observed by using Wavelet Power Spectrum (WPS) technique to study the storm H-component variation in greater detail by revealing the hidden patterns. This will lead to a deeper understanding of the storm-time at high latitude geomagnetic field variation. The geoelectric field $\boldsymbol{E}_H$, time derivatives of the North $\left(\frac{dx}{dt}\right)$, East $\left(\frac{dy}{dt}\right)$ and vertical $\left(\frac{dz}{dt}\right)$ component of the geoelectric field across the selected stations were considered and modeled. Wavelet Power Spectrum (WPS) was employed to study the fluctuations during the geomagnetic storms and the Ultra-Low Frequency (ULF) from the stations. It was noted that the WPS frequencies range between 0.05Hz – 0.4Hz within the intervals of 16-44Hrs respectively with the average powers of 200mm^2 – 2500mm^2. It was observed from Eskdalemuir that there was concentration of peak power around 16-24hrs and 36- 44hrs within the frequency band range between 0.15-0.25Hz, Lerwick displayed high power regions within 26 – 32hrs and 38-44Hrs which is 200mm^2-400mm^2 with the frequency of 0.25Hz. Nurmijärvi revealed the power maxima around 14-16hrs and 26 – 28hrs respectively within exceeding power of 1500 -2500mm^2 and frequency of 0.05 – 0.1Hz and Sodankylä and Sular depict the average power of 700mm^2 – 900mm^2 and 2500 mm^2 respectively, the frequencies bands were noted as 0.15Hz and 0.05-0.15Hz at Sodankylä and Sulari. Overall, the results confirm that geomagnetic storm effects were strongest, most persistent, and broadband at high latitudes, while becoming weaker, shorter-lived, and narrower in frequency toward mid- and low-latitudes. These findings highlight the critical role of auroral observatories in capturing storm-time magnetosphere–ionosphere dynamics, while mid- and low-latitude stations reflect the attenuation of geomagnetic disturbances with distance from the auroral oval.

Keywords: Intermagnet; Wavelet Power Spectrum; Geomagnetic storms; Magnetosphere; interplanetary magnetic field

1. Introduction

Geomagnetic storms are large-scale disturbances in the Earth's magnetosphere caused by interactions between the solar wind, interplanetary magnetic field (IMF), and Earth's magnetic field. These storms can disrupt satellite communications, navigation systems, power grids, and even human activities in space. In an era where technological systems form the backbone of daily life, understanding geomagnetic storms has become more critical than ever (Kappenman, 2005; Gopalswamy, 2006; Kamide & Chian, 2007).

The scientific study of geomagnetic storms dates back over 150 years. One of the earliest and most well-known events was the Carrington Event of 1859, which caused brilliant auroral displays worldwide and severely disrupted telegraph systems in Europe and North America (Boteler, 2006; Silverman, 2008; Clive et al., 2013). Later events, such as the 1921 New York Railroad Storm and the March 1989 storm that caused a nine-hour blackout in Quebec, Canada, demonstrated the potentially devastating impacts of these disturbances on modern infrastructure. More recently, the Halloween Storms of 2003 disrupted satellite operations, aviation communications, and GPS systems, highlighting the growing vulnerability of global society to space weather (Baker, 2008; Delores & Knipp, 2011; Jeffrey, 2018; Boteler, 2019).

The space age ushered in a new era of geomagnetic storm research. With the launch of satellites such as SOHO, ACE, and DSCOVR, and the establishment of global magnetometer networks, scientists gained

Bamidele, K. J., Falayi, F. C., Kotoye, A. A. Daini, P. A., and Martins, S. O., (2026). Variability Study of the Effect of Geomagnetic Storm of May, 10th - 11th, 2024 on the H-Component of the Geomagnetic Field using Wavelet Power Spectrum. *The Vocational and Applied Science Journal (VAS)*, vol. 20, no. 1, pp. 37-45.

access to near-real-time measurements of solar wind conditions and magnetic field variations. These observations revealed that geomagnetic storms are most commonly driven by coronal mass ejections (CMEs) and high-speed solar wind streams. Southward-directed IMF conditions were identified as a key factor in transferring energy from the solar wind into the magnetosphere through a process known as magnetic reconnection (NASA, 2015).

In recent decades, analytical methods have also advanced significantly. While early research relied heavily on statistical studies and linear approaches, the introduction of new mathematical techniques such as wavelet analysis has transformed the study of geomagnetic phenomena. Unlike Fourier transforms, which provide information about frequency but lose time localization, wavelets allow scientists to simultaneously examine signals in both time and frequency domains (Donald, et al., 200; Addison, 2002). This makes them highly effective for capturing sudden changes during storm onset, fluctuating peaks, and the gradual recovery phase. By applying wavelet analysis to geomagnetic indices such as the Dst index, researchers can better identify storm phases, detect transient variations, and link geomagnetic disturbances to their solar origins.

The study of geomagnetic storms is not only of scientific interest but also of strategic importance. Governments, space agencies, and power companies are increasingly concerned with space weather forecasting to protect critical infrastructure. Satellites provide continuous monitoring of solar wind parameters, while ground-based observatories track geomagnetic variations. The integration of these datasets enables the development of early warning systems, allowing operators of power grids, airlines, and navigation systems to take preventive measures against storm impacts. Despite significant advancements in our understanding of geomagnetic storms, accurately predicting their occurrence, intensity, and duration remains a significant challenge and the individual components of geomagnetic storms have been studied extensively, a comprehensive application of time–frequency methods to all aspects of a single storm event is limited. The primary aim of this study is to analyze the geomagnetic storms from May 10th - 11th 2024 in SULAR (Iceland), Sodankylä (Finland), Nurmijärvi (Finland), Lerwick (UK) and Eskdalemuir (UK) using Wavelet Power Spectrum. Numerous studies related to the effects of geomagnetic storms have been conducted for examples (Zhang *et al.,* 2007; Eastwood *et al.,* 2017; Falayi *et al.,* 2019; Adepitan & Falayi 2020; Arowolo *et al.,* 2021; Bolaji *et al.,* 2021; Ramirez *et al.,* 2023; Liu *et al.,* 2023; Chen *et al.,* 2024; Bamidele *et al.,* 2025). For the geomagnetic storms Prediction and Forecasting (Camporeale, 2019; Hapgood *et al.,* 2021;Murray *et al.,* 2022; Baker *et al.,* 2023; Mehta *et al.,* 2024). According to (Gonzalez, et al. 1994), geomagnetic storms are enormous disruptions of the Earth's magnetosphere caused by solar wind–magnetosphere interactions, especially during coronal mass ejections and high-speed solar wind streams. Auroral intensification, thermospheric expansion, and notable ionospheric irregularities in both hemispheres are caused at high latitudes by storm-time energy deposition due to particle precipitation and enhanced ionospheric currents (Daglis, et al., 1999; Schrijver & Siscoe, 2010). These mechanisms have a significant impact on navigation systems, satellite drag, and HF communication. Storm-enhanced density (SED), traveling ionospheric disturbances (TIDs), and disturbances in the Dst index driven by ring current intensification are all caused by geomagnetic storms at mid-latitudes (Kamide & Kusano, 2015). These effects can result in geomagnetically induced currents (GICs) that affect power transmission systems, especially in the Northern Hemisphere, though major consequences have been noticed in the Southern Hemisphere. At low latitudes**,** storm-time electric field penetration and disturbance dynamo effects modify the equatorial ionization anomaly (EIA), alter plasma distribution, and enhance scintillation activity, affecting GNSS reliability (Pulkkinen, A., 2007). Both hemispheres exhibit asymmetric responses due to seasonal, longitudinal, and conductivity differences, highlighting the complex global coupling between the magnetosphere, ionosphere, and thermosphere.

2. Materials and Methodology

Wavelet Power Spectrum (WPS) technique was utilized in analyzing the data acquired at a 1-second resolution using fluxgate magnetometers from the INTERMAGNET, as obtained by Tanskanen *et al.*, (2020). The study focuses on the investigation of geomagnetic storm using Wavelet power spectra from five distinct locations: Sulari (Iceland), Sodankylä (Finland), Nurmijärvi (Finland), Lerwick (UK) and Eskdalemuir (UK).

2.1 Computation of time derivative of geomagnetic field and geoeletric field

Equation 1 was used to obtain the time derivatives of the horizontal geomagnetic field, which gives estimates of the induction (Vijanen *et al.,* 2001).

$$\frac{dH}{dt} = \sqrt{(\frac{dBx}{dt})^2} + \sqrt{(\frac{dBy}{dt})^2} \quad (1)$$

dB_x/dt and dB_y/dt, respectively, represent the time derivatives of the east and north geomagnetic field components. The geoelectric field can be determined from variations in the geomagnetic field by applying the technique used by (Pirjola, 2002; Torta et al. 2014; Falayi et al., 2018), which considers the geomagnetic disturbance as a plane wave that propagates vertically downhill and an Earth with a uniform conductivity. Using this plane wave model, the north and east components of the geoelectric field Ex and Ey can be derived using Equations 2 and 3 in terms of the time derivative of the north geomagnetic field components Bx and By, respectively.

Published by The College of Vocational and Technology Education (COVTED), TASUED, vol. 20, no 1, pp. 37-45.

Figure 1: Map of the selected stations

Table 1: The Geographic and geomagnetic coordinate of the station considered

Station Name	Station Code	Location	Geographic Coordinate Latitude (^{0})	Geographic Coordinate Longitude (^{0})	Geomagnetic Coordinate Latitude (^{0})	Geomagnetic Coordinate Longitude (^{0})
Sular	SUL	Iceland	64.00^{0}W	21.00^{0}W	65.3^{0}W	65.3^{0}W
Sodankyla	SOD	Finland	67.37^{0}N	26.63^{0}E	64.1^{0}N	102.5^{0}E
Nurmijavi	NUR	Finland	60.51^{0}N	24.65^{0}E	57.3^{0}N	100.1^{0}E
Lerwick	LER	United Kingdom	60.15^{0}N	1.15^{0}W	57.5^{0}N	72.8^{0}W
Eskdalemuir	ESK	United Kingdom	55.31^{0}N	3.20^{0}W	52.7^{0}N	74.5^{0}W

$$E_x = \frac{1}{\sqrt{\pi\mu\sigma}} \int_0^\infty \frac{g(t-u}{\sqrt{u}}\, du, \quad g(t) = \frac{dBy(t)}{dt} \quad (2)$$

$$E_y = \frac{1}{\sqrt{\pi\mu\sigma}} \int_0^\infty \frac{g(t-u}{\sqrt{u}}\, du, \quad g(t) = \frac{dBx(t)}{dt} \quad (3)$$

where σ is the local ground conductivity and u is the Earth's magnetic permeability, which is 4 × 10-7 H/M. The north and east components of the geoelectric field are represented by Ex and Ey, respectively. The ground conductivity utilized in this study was obtained (Adam et al., 2012). Equation 4 can be used to compute the horizontal geoelectric field, $\boldsymbol{E_H}$.

$$E_H = \sqrt{(E_X)^2 + (E_X)^2} \quad (4)$$

2.2 Wavelet Power Spectrum Analysis

In wavelet analysis, the wavelet function's scale varies while maintaining a stable shape, influencing its effective dimension without affecting its fundamental form. This feature enables it possible to extract phase and amplitude information from time-localized characteristics. Wavelet-based spectrum estimations, as shown by Uchida et al. (2023), are similar to conventional Fourier spectra however, offer enhanced handling of non-stationary, anisotropic, or inhomogeneous data by offering localized insights in both time and space. It is essential to determining exactly any periodic signal's phase. In reality, a complex exponential wave and a Gaussian envelope are amplified to generate a Morlet wavelet, as demonstrated by the following mathematical relationship (Hafez and Ghamry, 2011).

$$\Psi 0(\eta) = \pi^{-\frac{1}{4}i\omega o\eta - \eta^2} \quad (5)$$

where Ψ0(η) is the wavelet value at non-dimensional time η, and ω_0 is the non-dimensional frequency. To be considered "admissible" as a wavelet in the preceding equation, the function needs to have a zero mean and be localized in both time and frequency space. This is the main wavelet function. A technique to change the wavelet's overall size and move it across time will now be required. Consequently, the equation below defines the 'scaled wavelets' (Han and Chang, 2013).

$$\varphi[\frac{(n^1-n)\,\partial}{s}] = (\frac{dt}{s})^{\frac{1}{2}}\, \varphi[\frac{(n^1-n)\,\partial}{s}] \quad (6)$$

where S denotes dilation variables applied to vary the scale and n denotes the translation variable employed to slide in time. As shown in equation 7 below (Richardson et al., 2002), the factor of $S^{\frac{-1}{2}}$ is a normalization function to keep the total energy of the scaled wavelet constant. Each of the values are separated by constant time interval dt.

$$(s) = \sum_{n^1=0}^{n=1} X_n \ \varphi*[\frac{(n^1-n)\delta t}{s}] \quad (7)$$

where the asterisk (*) represents complex conjugate. The above integral can be obtained for all values of n between the start and end dates, as well as for different values of the scales (typically assumed to be multiples of the lowest possible frequency). The wavelet amplitude and phase can then be plotted to obtain a two-dimensional image of the variability. A time series can then be divided into time-frequency phase space by applying a basic (mother) wavelet.

3. Results and Discussions

3.1 Results

Figures 2 – 6 displayed the wavelet power spectrum analysis to estimate the time-frequency variability on May 10th – 11th 2024 in Sulari (Iceland), Sodankylä (Finland), Nurmijärvi (Finland), Lerwick (UK) and Eskdalemuir (UK). The spectrum shows regions of varying power. Dark blue areas indicate low power, while red and yellow areas signify high power. The unit "mm" for power suggests that the spectrum might be related to meteorological or hydrological data, such as rainfall intensity or water level fluctuations, where "power" could represent the squared amplitude of these variations.

The y-axis represents a measure of frequency or scale ranging from approximately 0.05Hz to 0.4Hz, while the x-axis implicitly represents time, spanning the two-day (48hours) period. The color bar on the right indicates the power in millimeters (mm), ranging from 100 mm (dark blue) to 900 mm (dark red).

3.2 Discussions

The wavelet analysis of geomagnetic field variations over the 48-hour period from 00:00 UT 10 May 2024 to 23:59 UT 11 May 2024 reveals pronounced temporal and frequency-dependent behavior, underscoring the non-stationary nature of magnetospheric dynamics during moderate geomagnetic activity. The y-axis of the wavelet spectrum represents frequency, ranging from approximately 0.05 Hz to 0.4 Hz, while the x-axis covers the two-day window of continuous measurements. The color bar quantifies wavelet power in millimeters squared (mm^2), ranging from low-intensity dark blue (~100 mm^2) to high-intensity dark red (~900 mm^2), indicating the strength of oscillatory energy at given times and frequencies.

In Figure 2, several concentrated peaks in power are observed around 16–24 hours and 36–44 hours on both days, predominantly within 0.15–0.25 Hz. These features suggest the presence of recurring magnetospheric oscillations, possibly associated with substorm activity or periodic intensifications of the ring current. The periodicity corresponds to roughly 4–7 hours, consistent with the recurrence interval of magnetospheric pulsations (Pc5 range) that typically arise from field-line resonances or compressional waves transmitted from the solar wind (Ziesolleck & McDiarmid, 1994). The lowest mean power of 150 mm^2 and the highest range between 300 and 380 mm^2 indicate moderate disturbances within the geomagnetic field, likely reflecting fluctuating magnetospheric energy input.

The alternating zones of high and low power display a clear diurnal or semi-diurnal modulation. Such periodic enhancement aligns with the local solar-time dependence of ionospheric conductivity, which governs the coupling efficiency between solar wind forcing and magnetospheric currents (Kamide & Baumjohann, 1993). Hence, the observed wavelet patterns imply that diurnal variations in solar radiation modulate the magnetosphere's responsiveness, producing quasi-periodic power surges that repeat each day. The consistency of these oscillations across both days further supports a stable diurnal control rather than random fluctuations.

For the Lerwick station, distinct high-power regions are visible between 26–32 hours and 38–44 hours, corresponding to late May 10 and early May 11. These enhanced power zones suggest strong magnetospheric disturbances, possibly tied to southward turnings of the interplanetary magnetic field (IMF Bz) or transient solar-wind pressure enhancements. Increased power in this range signifies augmented geomagnetic activity, often associated with substorm expansions or auroral electrojet intensifications (Tsurutani & Gonzalez, 1997). Conversely, reduced power at higher frequencies (beyond 0.25 Hz) implies diminished small-scale fluctuations, consistent with the damping of high-frequency pulsations during storm recovery phases. Localized pockets of elevated power (~200–400 mm^2) around 38–40 hours at 0.25 Hz may represent short-lived Pi2 pulsations or storm-time compressional Pc4–Pc5 waves triggered by tail reconnection events.

During the early hours of May 10 (0–10 hours), the spectrum exhibits low power (~20–60 mm^2) across all frequencies, indicative of a quiet geomagnetic field prior to the arrival of a significant solar-wind disturbance. Power intensifies as the day progresses, peaking toward the latter half of May 10 and early May 11. This temporal evolution likely marks the main phase of a geomagnetic storm, when energy transfer from the solar wind into the magnetosphere increases through enhanced reconnection at the dayside magnetopause (Dungey, 1961; Pulkkinen *et al.,* 2016) (See Figure 3).

In Figure 4, the emergence of strong, localized power maxima around 14–16 hours, 26–28 hours, and 38–40 hours each exceeding 1,500–2,500 mm^2 in the 0.05–0.1 Hz band signals intense, low-frequency oscillations corresponding to large-scale magnetospheric reconfigurations. Such low-frequency components are typical of Pc5 pulsations associated with global cavity modes or Kelvin–Helmholtz surface waves at the magnetopause boundary (Mann, *et al.,* 1999). These peaks indicate that the system was driven by solarwind

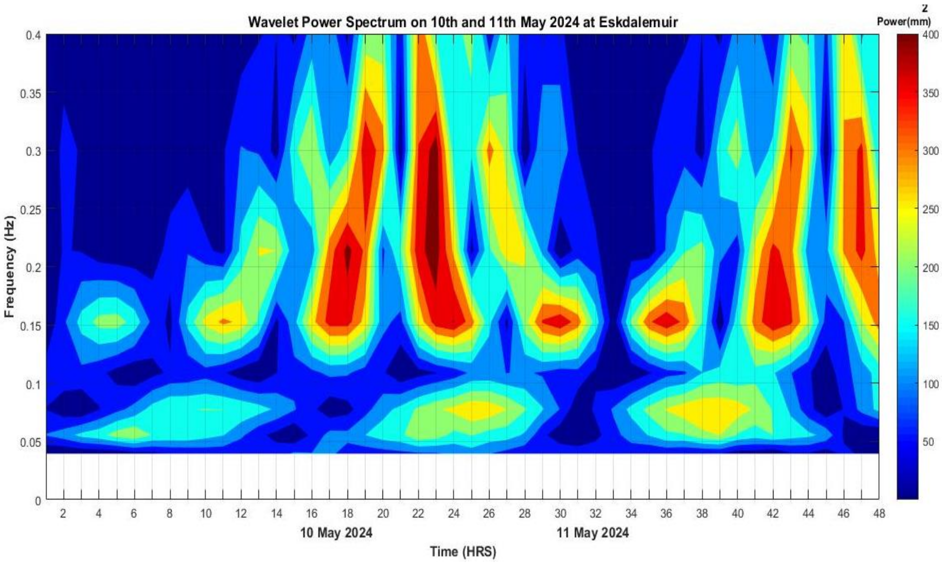

Figure 2: wavelet power spectrum of Eskdalemuir

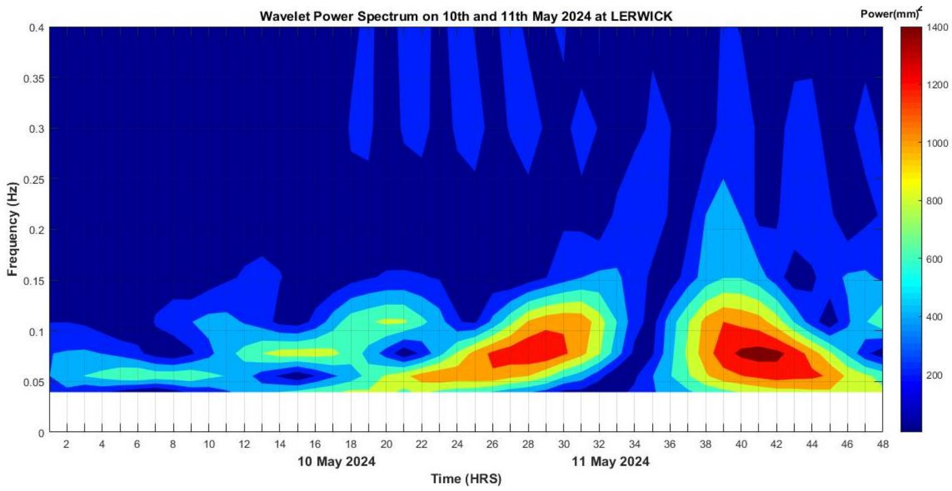

Figure 3: wavelet power spectrum of Lerwick

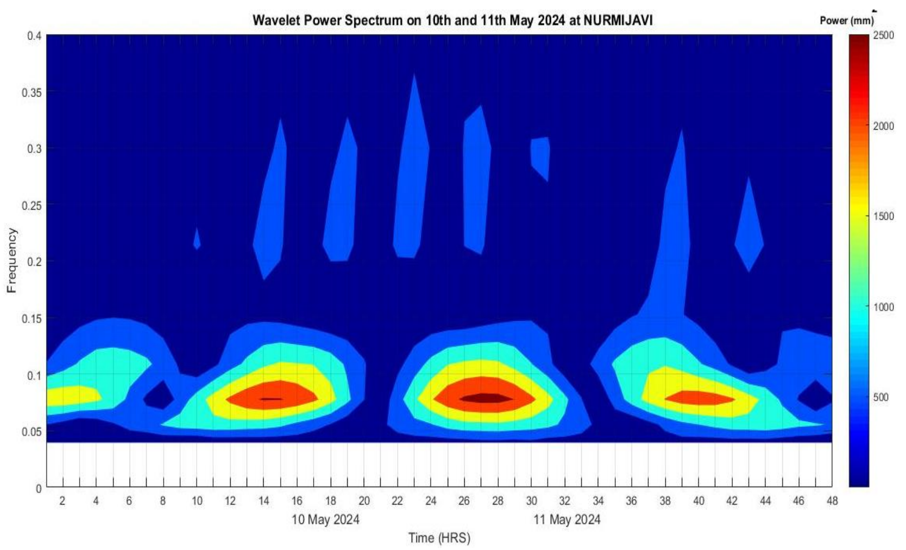

Figure 4: wavelet power spectrum of Nurmijvi

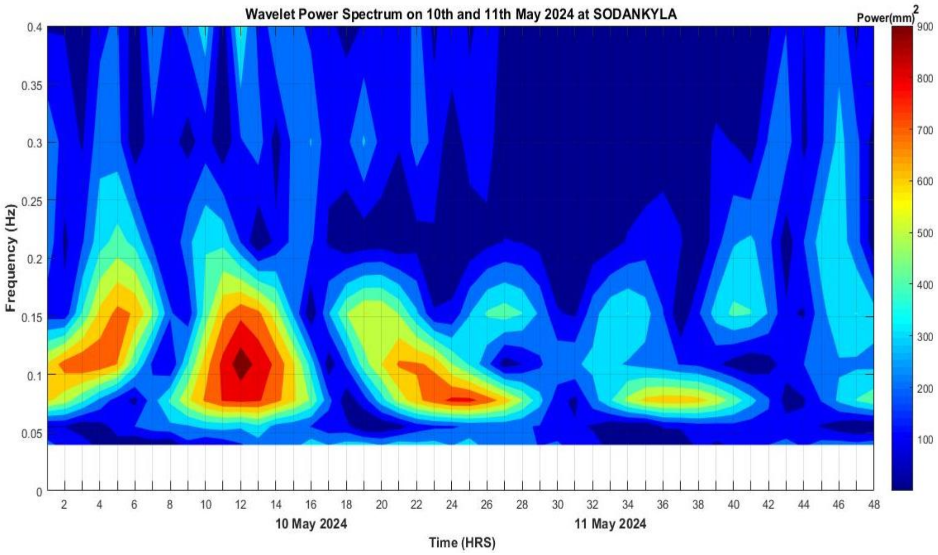

Figure 5: wavelet power spectrum of Sodankyla

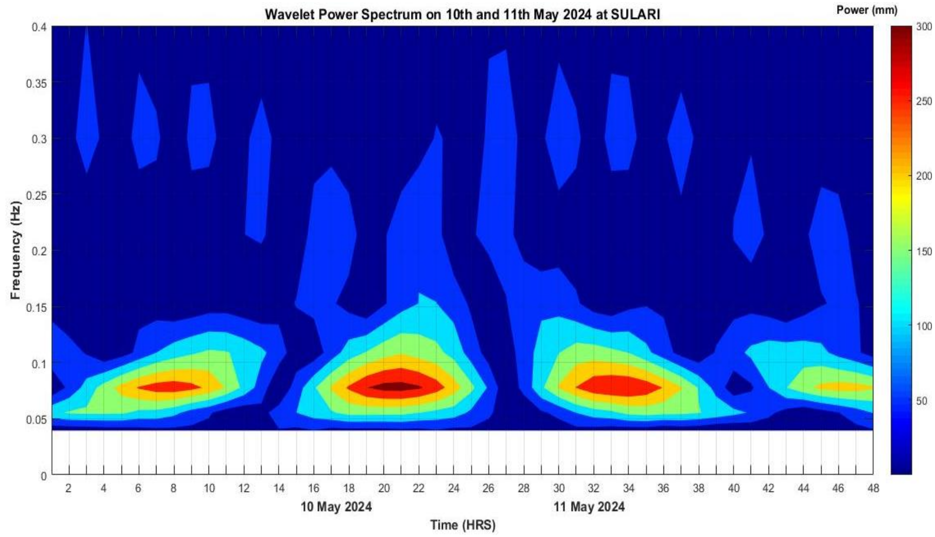

Figure 6: wavelet power spectrum of Sulari

dynamic pressure fluctuations or IMF changes, causing periodic energy injections into the magnetosphere. The presence of discrete bursts at specific times rather than a continuous high-power band demonstrates the non-stationary character of geomagnetic fluctuations, reflecting transient processes such as substorm onsets and ring-current intensifications (Kamide & Rostoker, 2004).

Between these high-power episodes, extended regions of reduced intensity (dark blue) reveal quieter magnetospheric intervals, implying temporary stabilization following energy release events. The alternation between active and calm phases supports the concept of self-organized criticality within the magnetosphere, where small perturbations can initiate rapid reorganizations followed by relaxation (Chang, 1999). The wavelet representation captures this behavior more effectively than Fourier analysis, as it simultaneously resolves the evolution of power across time and frequency (Torrence & Compo, 1998).

In Figure 5, the spectrum highlights two major bursts of energy 700–900 mm² around 11–15 hours on May 10 and 20–22 hours on May 11, concentrated near 0.15 Hz. These episodes reflect discrete energy injections into the magnetosphere, probably linked to substorm activity or sudden impulses following interplanetary shocks. The "blobs" of high power correspond to temporally localized disturbances, confirming that geomagnetic oscillations are event-driven rather than continuous. The asymmetry between the two days further suggests variability in solar-wind driving conditions. Such episodic enhancements are consistent with results from the SuperMAG and OMNI datasets during storm-time intervals, where enhanced solar-wind velocity and IMF Bz variability directly modulate ground magnetic power spectra (Yizengaw *et al.*, 2020).

Moreover, the spectrum demonstrates that both the power amplitude and dominant frequency evolve dynamically across the 48-hour window, reinforcing the non-stationary and multiscale nature of geomagnetic fluctuations. These time-localized oscillations coincide with known magnetospheric pulsation ranges, confirming that wavelet analysis effectively identifies transient wave packets and diurnal periodicities that classical spectral methods often miss (De Michelis *et al.,* 2005).

The Sulari station results (Figure 6) exhibit three pronounced peaks in wavelet power at 6–10 hours, 20–24 hours, and 31–34 hours, with intensities of 250–300 mm² in the 0.05–0.15 Hz band. These peaks correspond to large-scale oscillations of the geomagnetic field, characteristic of auroral electrojet intensifications or field-aligned current enhancements during substorm growth and expansion phases. Between these maxima, power values drop to moderate levels (100–150 mm²), marking quieter intervals. Isolated low-power patches at 8–12 hours and 20–22 hours suggest localized weakening of geomagnetic activity, possibly linked to temporary northward IMF Bz conditions that reduce magnetospheric convection.
Taken together the spectra from all stations reveal that the magnetospheric system underwent multiple, temporally separated energy injections over the two-day period, accompanied by short relaxationintervals. The dominant frequencies (0.05–0.25 Hz) correspond to magnetohydrodynamic (MHD) pulsations driven by solar-wind variability, while the diurnal recurrence underscores the coupling between magnetospheric and ionospheric processes modulated by solar illumination. These findings confirm that geomagnetic field variations are inherently multiscale and non-stationary with energy distributed intermittently in both time and frequency domains.

Wavelet analysis thus provides a powerful diagnostic for distinguishing between continuous background fluctuations and discrete geomagnetic events. The spatial consistency between stations (e.g., Lerwick and Sulari) implies that many of the detected features are of global magnetospheric origin rather than purely local disturbances. Overall, the 48-hour wavelet spectra demonstrate how short-term solar-wind variations and diurnal ionospheric modulation jointly control the morphology of geomagnetic field oscillations, validating previous studies on magnetospheric wave coupling and temporal intermittency (Vörös *et al.,* 2002; Moldwin & Hughes, 1994).

The wavelet power spectrum analysis of the geomagnetic storm of May 10–11, 2024, revealed distinct temporal and spatial variations in geomagnetic activity across the analyzed stations. The differences observed among BUDVOK, Lerwick, and Sulari underscore the latitude-dependent response of the magnetosphere–ionosphere system to solar wind forcing. At BUDVOK, geomagnetic activity manifested as short, intense bursts primarily within the Pc4–Pc5 ultra-low frequency (ULF) band (0.05–0.1 Hz) , a frequency range typically associated with magnetospheric field line resonances (FLRs) and substorm current systems (Vellante *et al.,* 2004; Villante & Di Giuseppe, 2004). In contrast, Lerwick exhibited moderate but recurrent peaks, displaying semi-diurnal oscillations likely linked to global magnetospheric compressions induced by solar wind dynamic pressure variations (Villante & Di Giuseppe, 2004; Daglis *et al.,* 1999).

At Sulari (Iceland), the strongest power concentrations reaching up to 2,500 mm² indicate the presence of highly energetic fluctuations associated with auroral electrojet intensification and substorm expansion phases (Baker *et al.,* 1996; Kennel *et al.,* 1992). These peaks correspond to strong energy transfer from the solar wind into the magnetosphere, driven by enhanced interplanetary magnetic field (IMF) southward turning and increased solar wind velocity, which are known to trigger auroral activity and ring current enhancement (Abdu & Brum, 2018; Daglis *et al.,* 1999).

The observed differences among stations confirm that geomagnetic storms are highly non-uniform phenomena, influenced by latitude, magnetic local time, and ionospheric conductivity. High-latitude stations (such as Sulari and Lerwick) consistently recorded broader frequency responses and longer disturbance durations, whereas mid-latitude sites like BUDVOK experienced intermittent, less persistent pulsations. These results agree with the established understanding that auroral zone stations are directly coupled to the magnetospheric substorm current wedge , while mid-latitude stations primarily record the ground-projected signatures of large-scale magnetospheric compressions (Mourenas *et al.,* 2019; Vörös *et al.,* 2002).

The wavelet analysis technique was particularly effective in this investigation, as it captured the non-stationary and multi-scale nature of geomagnetic storm fluctuations. This method enables precise identification of transient spectral features, distinguishing between continuous storm phases and short-lived substorm injections (Torrence & Compo, 1998; Balasis *et al.,*2018). The results corroborate prior studies that demonstrated the suitability of wavelet transforms for detecting localized energy enhancements and temporal evolution of magnetospheric processes during disturbed conditions (Chang, 1999; Vassiliadis *et al.,* 1995).

4. Conclusions

Overall, the findings confirm that geomagnetic storm impacts vary systematically with latitude, with high-latitude regions exhibiting greater oscillation power, broader frequency bands, and longer recovery times compared to mid-latitude stations. This gradient is consistent with the physics of magnetospheric coupling, where enhanced field-aligned currents and plasma instabilities dominate the auroral zones. The study thus reinforces the importance of wavelet-based spectral diagnostics as a robust tool for characterizing geomagnetic storm morphology and for improving our understanding of solar wind–magnetosphere–ionosphere coupling dynamics.

References

Abdu, M. A., & Brum, C. G. M. (2018). Electrodynamics of ionospheric perturbations during geomagnetic storms. Journal of Atmospheric and Solar-Terrestrial Physics, 171, 29–43.

Adam, A., Prácser, E., & Wesztergom, V. (2012). Global 1-D modelling of magnetotelluric responses for GIC studies. Acta Geodaetica et Geophysica Hungarica, 47(4), 377–387.

Adepitan, A. O., & Falayi, E. O. (2020). Statistical analysis of geomagnetic storm occurrence and intensity during solar cycles 23 and 24. Advances in Space Research, 66(2), 314–323.

Addison P S. (2002). *The Illustrated Wavelet Transform Handbook*. Institute of Physics Publishing

Arowolo, O. M., Bolaji, O. S., & Adebesin, B. O. (2021). Interplanetary drivers of intense geomagnetic storms and their effects on the African ionosphere. Space Weather, 19(10), e2021SW002895.

Baker, D. N., Pulkkinen, A., & Daglis, I. A. (2023). Extreme geomagnetic storms and their technological impacts: An international assessment. Space Weather, 21(3), e2022SW003410.

Baker, D. N., Pulkkinen, T. I., Angelopoulos, V., Baumjohann, W., & McPherron, R. L. (1996). Neutral line model of substorms: Past results and present view. Journal of Geophysical Research: Space Physics, 101(A6), 12975–13010.

Balasis, G., Donner, R. V., Potirakis, S. M., & Daglis, I. A. (2018). Magnetospheric dynamics and chaos: The role of nonlinear processes. Nonlinear Processes in Geophysics, 25(2), 237–250.

Bolaji, O. S., Oladipo, O. A., & Adebesin, B. O. (2021). Impact of the August 25–26, 2018 geomagnetic storm on ionospheric total electron content in American and Asian-Australian sectors. Journal of Atmospheric and Solar-Terrestrial Physics, 217, 10562.

Boteler, D. H. (2006). The super storms of August/September 1859 and their effects on the telegraph system. *Advances in Space Research*, 38, 159–172.

Borovsky, J. E. (2018). Solar wind and magnetosphere coupling: The role of IMF orientation. Journal of Atmospheric and Solar-Terrestrial Physics, 179, 204–218.

Boteler, D. H. (2019). A 21st-century view of the March 1989 magnetic storm. *Space Weather*, 17, 1427–1441.

Bamidele, K. J, Adelaja, A.D. Fowodu, T.O. Kotoye, A.A. Ajose, A.S. Falayi, F.C. Falayi, E.O. (2025). Quantitative Analysis of Geomagnetic Indices Using Wavelet Power Spectrum. *Nigerian Journal of Environmental Sciences and Technology*, 9(1), pp. 105-115.

Camporeale, E. (2019). The challenge of machine learning in space weather: Nowcasting and forecasting. Space Weather, 17(8), 1166–1207.

Chang, T. (1999). Self-organized criticality, multi-fractal spectra, and intermittency in space plasmas. Physics of Plasmas, 6(11), 4137–4145.

Clive D. Beggan, A. W. P. Thomson, & B. W. McKay (2013). The Carrington event: The largest magnetic storm on record. *Geophysical Research Letters*, 40, 1–6.

Chen, Y., Zhang, X., & Li, H. (2024). Ionospheric scintillation effects on GNSS signals during intense geomagnetic storms: A multi-constellation analysis. Journal of Geodesy, 98(2), 24–39.

Baker, D. N. (2008). Severe space weather events—Understanding societal and economic impacts: A workshop report. *National Academies Press*, Washington, DC.

Daglis, I. A., Thorne, R. M., Baumjohann, W., & Orsini, S. (1999). The terrestrial ring current: Origin, formation, and decay. Reviews of Geophysics, 37(4), 407–438.

De Michelis, P., Consolini, G., & Marchetti, M. (2005). Multiscale features of the storm-time magnetosphere. Journal of Geophysical Research: Space Physics, 110(A12), A12213.

Donald B. P. & Andrew T. W. (2000). *Wavelet Methods for Time Series Analysis*. Cambridge University Press

NASA, NOAA, & U.S. Air Force (2015). Real-time solar wind and IMF observations for space weather monitoring.

Eastwood, J. P., Biffis, E., Hapgood, M. A., Green, L., Bisi, M. M., Bentley, R. D., & Dalla, S. (2017). The economic impact of space weather: Where do we stand? Risk Analysis, 37(2), 206–218.

Falayi, E. O., Bolaji, O. S., & Adebesin, B. O. (2019). Effects of geomagnetic storms on the horizontal (H) component of the Earth's magnetic field at high and low latitudes. Annales Geophysicae, 37(3), 345–357.

Falayi, E. O., Rabiu, A. B., & Adebesin, B. O. (2018). Estimation of geoelectric field variations during geomagnetic disturbances in the equatorial region. Journal of Atmospheric and Solar-Terrestrial Physics, 171, 92–102.

Hafez, A. G., & Ghamry, E. (2011). Application of Morlet wavelet transform for spectral analysis of geomagnetic pulsations. Annales Geophysicae, 29(12), 2327–2337.

Han, D., & Chang, T. (2013). On the properties and applications of scaled wavelets in geophysical signal analysis. Nonlinear Processes in Geophysics, 20(6), 1027–1038.

Hapgood, M., Knipp, D., & Pulkkinen, T. (2021). International collaboration in space weather forecasting: Current status and future directions. Space Weather, 19(6), e2021SW002894.

Kamide, Y., & Rostoker, G. (2004). What is a geomagnetic substorm? Eos, 85(4), 61–68.

Kamide, Y. & Kusano, K. (2015). *No major solar flares but the largest geomagnetic storm in the present solar cycle.* Space Weather, 13(6), 365–367.

Knipp, D. J., Fraser, B. J., & Redmon, R. J. (2021). Impacts of geomagnetic storms on satellite systems: Mechanisms, risks, and mitigation strategies. Reviews of Geophysics, 59(4), e2020RG000725.

Liu, X., Wang, W., & Burns, A. (2023). Modeling thermospheric heating and expansion during geomagnetic storms: Implications for satellite drag. Journal of Geophysical Research: Space Physics, 128(1), e2022JA031277.

Mehta, A., Ridley, A., & Pulkkinen, A. (2024). Data assimilation techniques for real-time geomagnetic storm forecasting. Journal of Space Weather and Space Climate, 14, 20.

Mourenas, D., Artemyev, A. V., Agapitov, O. V., & Krasnoselskikh, V. V. (2019). Time evolution of electron fluxes during geomagnetic storms driven by auroral kilometric radiation. Journal of Geophysical Research: Space Physics, 124(7), 5349–5367.

Murray, S., Arge, C., & Reiss, M. (2022). Ensemble forecasting of geomagnetic storms: Combining models to improve accuracy. Space Weather, 20(5), e2021SW002973.

Pirjola, R. (2002). Review on the calculation of surface electric and magnetic fields and of geomagnetically induced currents in ground-based technological systems. Surveys in Geophysics, 23(1), 71–90.

Pulkkinen, A., Rastätter, L., Kuznetsova, M., & Hesse, M. (2016). Geomagnetic storms—Causes, effects and prediction. Space Weather, 14(7), 473–475.

Pulkkinen, A. (2007). *Space weather: Terrestrial perspective.* Living Reviews in Solar Physics, 4(1), 1.

Ramirez, J., et al. (2023). Resilience of global power grids to geomagnetic storms: A decade-long assessment (2013–2022). Space Weather, 21(8), e2023SW003456.

Richardson, J. D., Paularena, K. I., Wang, C., & Burlaga, L. F. (2002). The solar wind and geomagnetic activity: Wavelet transform analysis of time series data. Geophysical Research Letters, 29(12), 1619.

Silverman, S. A. (2008). Low-latitude auroras: The storm of 1–2 September 1859. *Journal of Atmospheric and Solar–Terrestrial Physics*, 70, 1301–1308.

Tanskanen, E. I., et al. (2020). High-resolution (1-second) fluxgate magnetometer observations for geomagnetic research and applications. Earth, Planets and Space, 72(1), 45.

Torrence, C., & Compo, G. P. (1998). A practical guide to wavelet analysis. Bulletin of the American Meteorological Society, 79(1), 61–78.

Torta, J. M., Marcuello, A., Campanyà, J., & Gaya-Piqué, L. R. (2014). Improved modelling of geomagnetically induced currents in Spain: Influence of deep lithospheric structures. Earth, Planets and Space, 66, 152.

Tsurutani, B. T., & Gonzalez, W. D. (1997). The interplanetary causes of magnetic storms: A review. In Magnetic Storms (Geophysical Monograph 98) (pp. 77–89). American Geophysical Union.

Uchida, H., et al. (2023). Wavelet-based spectral analysis for geophysical signals: Comparisons with Fourier methods and applications to non-stationary data. Journal of Geophysical Research: Space Physics, 128(2), e2022JA031234.

Vassiliadis, D., Sharma, A. S., Eastman, T. E., & Papadopoulos, K. (1995). Low-dimensional chaos in magnetospheric activity from AE time series. Geophysical Research Letters, 22(9), 1193–1196.

Vellante, M., Lühr, H., Zhang, T. L., Wesztergom, V., Villante, U., De Lauretis, M., Piancatelli, A., Rother, M., Schwingenschuh, K., Koren, W., & Magnes, W. (2004). Ground/satellite signatures of field line resonance: A test of theoretical predictions. Journal of Geophysical Research: Space Physics, 109, A06210.

Vörös, Z., Baumjohann, W., Nakamura, R., Runov, A., Volwerk, M., Zhang, T. L., Klecker, B., Rème, H., & Balogh, A. (2002). Multi-scale magnetic field intermittence in the plasma sheet. Annales Geophysicae, 20(2), 367–374.

Yizengaw, E., Zesta, E., Komjathy, A., & Mannucci, A. J. (2020). Storm-time ionospheric disturbances and their relation to solar-wind conditions. Journal of Geophysical Research: Space Physics, 125(1), e2019JA027691.

Zhang, J., Richardson, I.G., Webb, D.F., Gospalswamy, N., Huttunen, E, Kasper, J.C., Nitta, N.V., Poomvises, W., Thompson, B.J., Wu, C.C., Yashiro, S. & Zhukov, A.N (2007).. Solar and interplanetary sources of major geomagnetic storms (Dst ≤ -100 nT) during 1996–2005. Journal of Geophysical Research: Space Physics, 112(A10), A10102.

Kappenman J. (2005). An overview of the impacts of geomagnetic storms on electric power systems. *IEEE Power Engineering Society General Meeting*, 1–6.

Kamide, Y. & Chian, A. (2007). *Handbook of the Solar–Terrestrial Environment*. Springer

Gopalswamy Nat (2006). Coronal mass ejections and space weather. *Space Science Reviews*, 124, 145–168.